Opto-Electronic Advances

Supplementary information

April 2024, Vol. 7, No. 4

DOI: 10.29026/oea.2024.230194

Ultrahigh performance passive radiative cooling by hybrid polar dielectric metasurface thermal emitters

Yinan Zhang[1†*], Yinggang Chen[1,2†], Tong Wang[1†], Qian Zhu[1] and Min Gu[1*]

[1]Institute of Photonic Chips, University of Shanghai for Science and Technology, Shanghai 200093, China; [2]Centre for Artificial-Intelligence Nanophotonics, School of Optical-Electrical and Computer Engineering, University of Shanghai for Science and Technology, Shanghai 200093, China.

[†]These authors contributed equally to this work.

*Correspondence: YN Zhang, E-mail: zhangyinan@usst.edu.cn; M Gu, E-mail: gumin@usst.edu.cn

This file includes:

Supplementary information for this paper is available at https://doi.org/10.29026/oea.2024.230194

Section 1: Machine learning inverse design

The neural network used for machine learning was a fully connected perception neural network with four hidden layers. The neuron numbers of per layer was 200, 200, 250 for the 2-, 3-, and 4-layer metasurface structures. The input of the network was the structure parameters (the height of SiO_2 and Si_3N_4, the diameter of the cylinder, and the cylinder space) within the range of 0–10 μm, and the output was 261 emission spectrum sampled points between 3 and 16 μm. The Relu activation function was employed after each hidden layer. The loss function was the mean square error between each point on the spectrum and the 261-dimensional output of the neural network. Meanwhile, RMSPropOptimizer was selected to optimize all weights and biases. The FDTD method was used to generate a certain amount of sample data (sample size of 2-, 3- and 4-layers structure corresponds to 5000, 5000 and 10000 respectively). The time expenditure of generating 10000 sample data is around 133.5 h by using a workstation with a 3.6-GHz Intel Xeon W-2133 processor. We split the data into three categories: train, validation, and test according to the ratio of 8:1:1. The batch size of the training data was 100. After 10 iterations of the training set, one validation was carried out to adjust the network hyperparameters. Table S1 summarizes the neural network architecture parameters and cross-validation results for various cases. For the inverse design, the neural network was firstly trained so that it can predict the spectrum with given parameters of the metasurfaces. Then, the weights of the network were fixed, and the input of the structure parameters was set as trainable variable and back propagation was used to train the inputs of the network using a loss function defined as mean square error between the output and the ideal emission spectrum.

Section 2: Cooling power and emissivity calculation

The cooling power of the radiative cooler was calculated by using the following equation.

$$P_{\text{cooing}}(T) = P_{\text{rad}}(T) - P_{\text{atm}}(T_{\text{a}}) - P_{\text{sun}} - P_{\text{conv+cond}} \ , \tag{S1}$$

where P_{rad} is the radiative power of the thermal emitters; P_{atm} and P_{sun} are the power absorbed from the atmosphere and the sun; $P_{\text{conv+cond}}$ is the heat gain from environment by non-radiative heat exchange.

$$P_{\text{rad}}(T) = A\int \mathrm{d}\Omega\cos\theta\int_0^{\infty}\mathrm{d}\lambda I_{\text{BB}}(T,\lambda)\,\varepsilon(\lambda,\theta) \ , \tag{S2}$$

$$P_{\text{atm}}(T_{\text{a}}) = A\int \mathrm{d}\Omega\cos\theta\int_0^{\infty}\mathrm{d}\lambda I_{\text{BB}}(T_{\text{a}},\lambda)\varepsilon(\lambda,\theta)\,\varepsilon_{\text{atm}}(\lambda,\theta) \ , \tag{S3}$$

$$P_{\text{sun}} = A\int_0^{\infty}\mathrm{d}\lambda\varepsilon(\lambda,\theta_{\text{sun}})\,\mathrm{I}_{\text{AM1.5}}(\lambda) \ , \tag{S4}$$

$$P_{\text{conv+cond}} = Ah(T_{\text{a}} - T) \ . \tag{S5}$$

Here, A is the surface area of the object and $\int \mathrm{d}\Omega = 2\pi\int_0^{\frac{\pi}{2}}\mathrm{d}\theta\sin\theta$ is the integration of a hemispherical. $I_{\text{BB}}(T,\lambda)$ is black-body thermal radiation at temperature T. $\varepsilon(\lambda,\theta)$ is the emissivity of the object at the wavelength λ and emission angle θ and $\varepsilon_{\text{atm}} = 1 - t(\lambda)^{1/\cos\theta}$ represents the emissivity of the atmosphere, where $t(\lambda)$ is the transmittance of the atmosphere in the zenith direction. $I_{\text{AM1.5}}(\lambda)$ represents the AM 1.5 solar irradiation and h is the non-radiative heat exchange coefficient, including heat conduction h_{conv} and heat convection h_{cond}, respectively.

The average emissivity was calculated by weighting the spectra to the corresponding blackbody thermal emission. The spectral selectivity was calculated as the ratio of average emissivity within the atmospheric transparency window to that across the entire measured thermal wavelength range.

Supplementary Figures

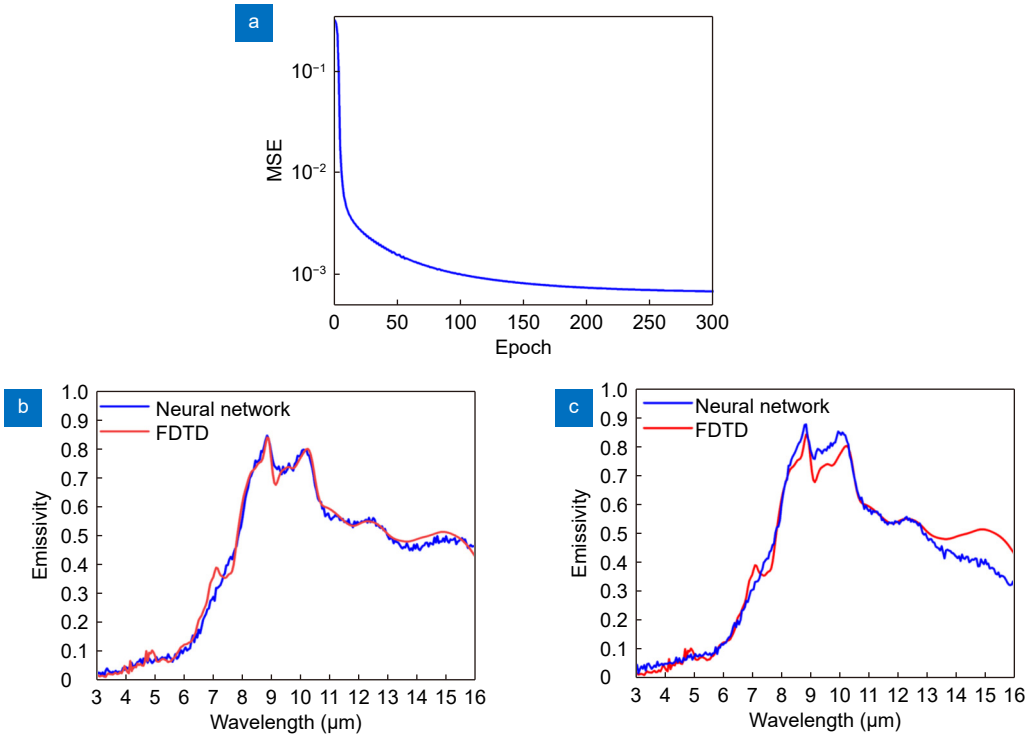

Fig. S1 | (**a**) Mean Square Error (MSE) for the 2-layer configuration training. (**b**) Comparison of the spectrum predicted by the neural network and calculated by FDTD simulation for a 2-layer configuration. (**c**) Comparison of the spectrum by inversely designed structure and the structure calculated by FDTD simulation for the 2-layer configuration.

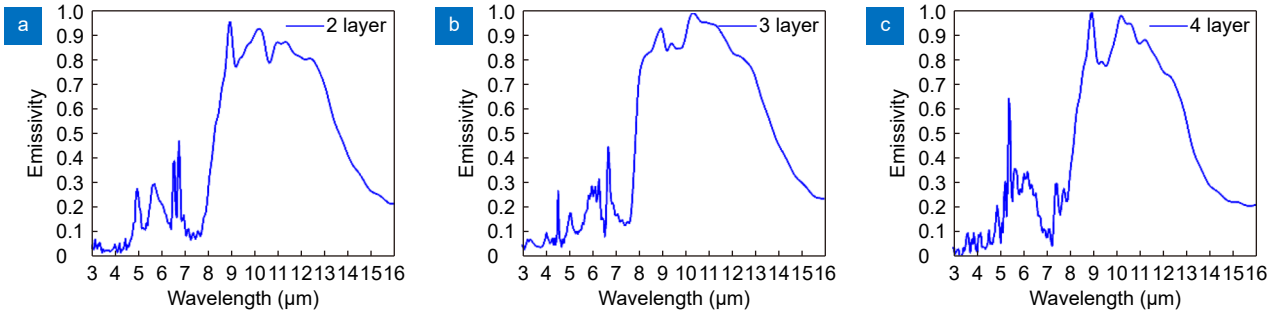

Fig. S2 | Thermal emission spectra produced by using the neural network inverse design method for various layer metasurface configurations.

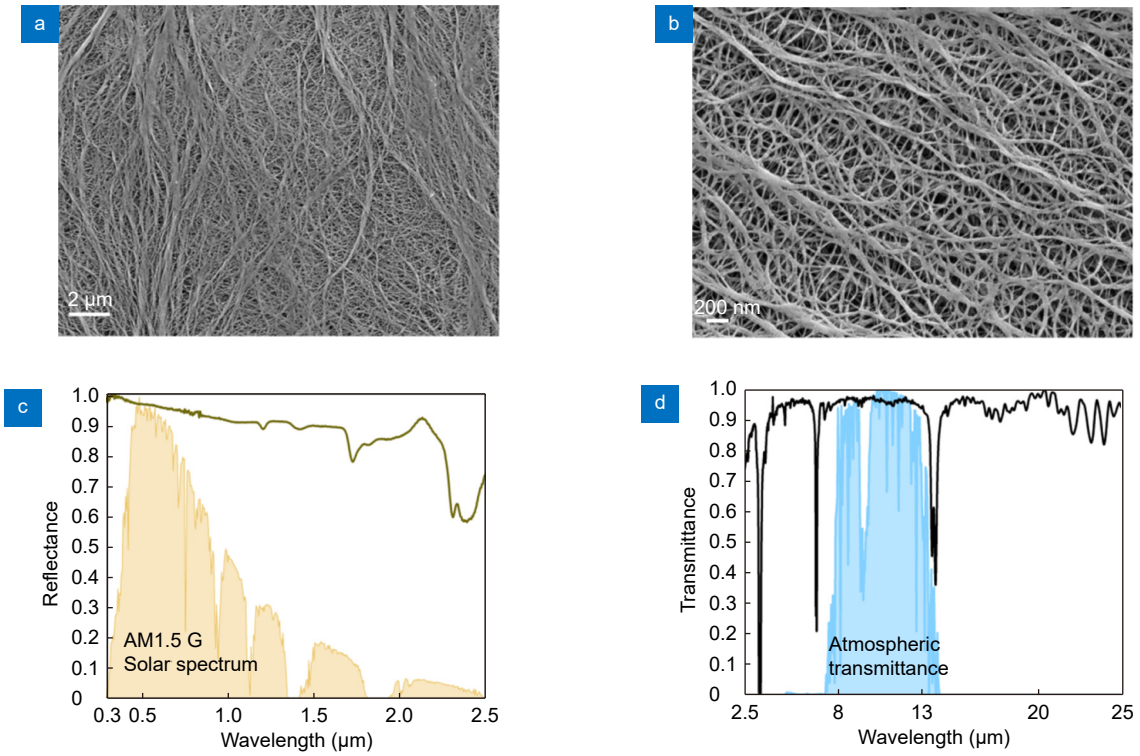

Fig. S3 | Characterizations of the home-made nanoporous solar reflector. (**a**, **b**) SEM images of the materials (scale bar: 2 μm and 200 nm for (a) and (b), respectively). (**c**) Reflection in the solar wavelength range of the nanoporous PE integrated with the metasurface thermal emitter. (**d**) Infrared transmission spectra of the nanoporous PE.

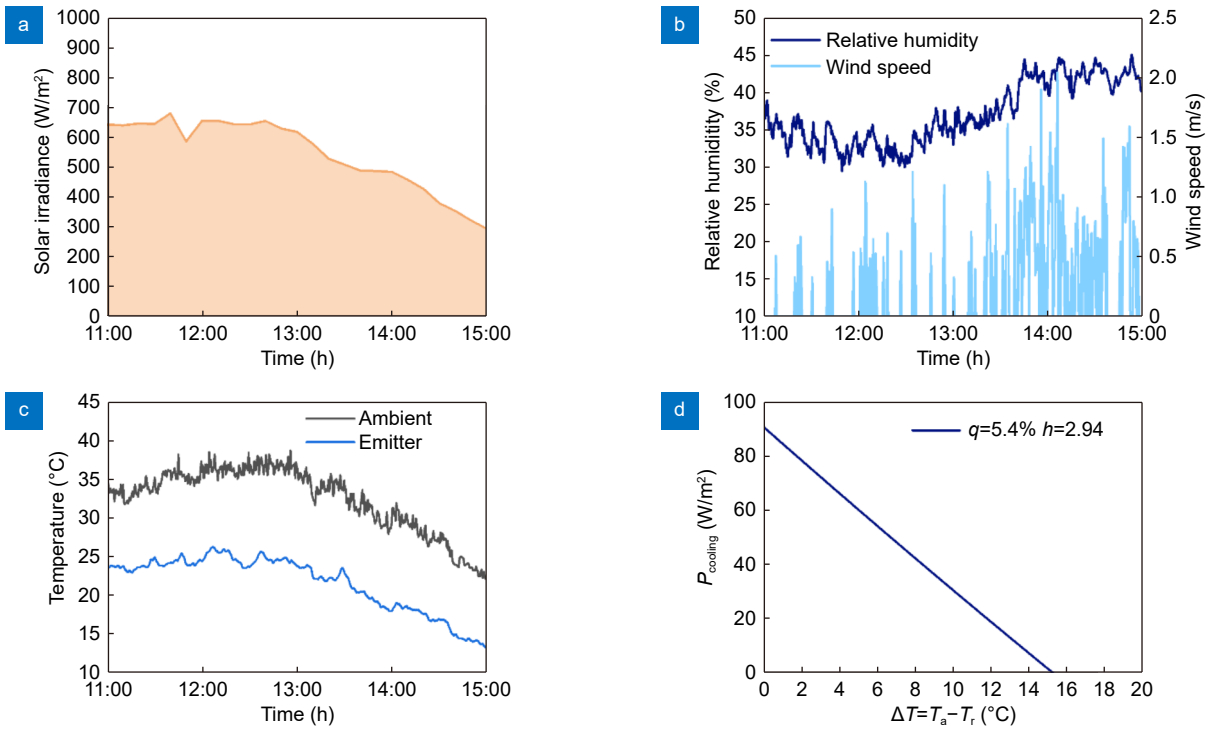

Fig. S4 | Rooftop test results during the winter days. (**a**, **b**) The solar irradiation and environment (wind speed and relative humidity) during the rooftop test. (**c**) Steady-state temperature of the metasurface radiative cooler. (**d**) The net cooling power of the cooler with temperature reduction using the experimental spectral data.

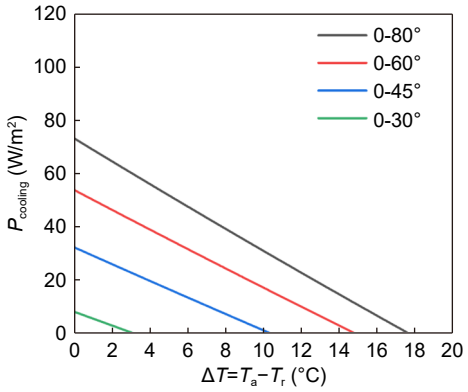

Fig. S5 | Net cooling power of our radiative cooler with various angle restriction during the summertime in Shanghai, China with an average ambient temperature of 307 K. The solar absorption and the heat exchange coefficient were set as 2% and 2 Wm^{-2} K^{-1}, respectively.

Table S1 | Neural network architecture and cross-validation results for various cases.

Layer	Neurons per layer	MRE (train)	MRE (val)	MRE (test)
2	200	0.131%	0.259%	0.079%
3	200	0.103%	0.179%	0.093%
4	225	0.155%	0.398%	0.114%

Table S2 | Cooling performance of our results, compared with state-of-the-art results.

Materials	Structure	Solar reflectance	Thermal emittance	Type of radiator	Maximum Temperature drop (°C)	Year
This work	Machine learning mediated hybrid metasurface	0.95	0.92	Selective	15.4	2023
PS/PDMS/PECA (ref.[S12])	Hierarchical porous polymer	0.96	0.95	Broadband	12.9	2022
SiO_2/SiOxNy/ Ti/Ag (ref.[S11])	Multilayer inorganic film	0.964	0.85	Selective	5	2022
PEO （ref.[S10]）	Hierarchical nanofibres	0.963	0.78	Selective	5	2021
PMMA (ref.[S9])	Micropore array/Random nanopores	0.95	0.98	Broadband	8.9	2021
PDMS/Al_2O_3 (ref.[S8])	Photonic structure	0.95	0.96	Broadband	5.1	2020
PVDF/TEOS /SiO_2 (ref.[S7])	Photonic structure	0.97	0.96	Broadband	<6	2019
Wood (ref.[S6])	Mechanical pressed and porous structure	0.96	-	Broadband	4	2019
P(VdF–HFP) (ref.[S5])	Hierarchical porous polymer	0.96	0.97	Broadband	6	2018
Si(phosphorous-doped n-type)/Ag (ref.[S4])	Metasurfaces	-	-	Selective	7.36 (theoretically)	2017
TPX/SiO_2/Ag (ref.[S3])	Metamaterial	0.96	>0.93	Broadband	-	2017
Ge/Al (ref.[S2])	Metamaterial	-	0.90	Selective	9 (theoretically)	2015
SiO_2/HfO_2/Ag (ref.[S1])	Multilayer thin films	0.97	-	Selective	4.9	2014

References

S1. Raman AP, Anoma MA, Zhu LX et al. Passive radiative cooling below ambient air temperature under direct sunlight. *Nature* **515**, 540–544 (2014).

S2. Hossain MM, Jia BH, Gu M. A metamaterial emitter for highly efficient radiative cooling. *Adv Opt Mater* **3**, 1047–1051 (2015).

S3. Zhai Y, Ma YG, David SN et al. Scalable-manufactured randomized glass-polymer hybrid metamaterial for daytime radiative cooling. *Science* **355**, 1062–1066 (2017).

S4. Zou CJ, Ren GH, Hossain MM et al. Metal-Loaded dielectric resonator metasurfaces for radiative cooling. *Adv Opt Mater* **5**, 1700460 (2017).

S5. Mandal J, Fu YK, Overvig AC et al. Hierarchically porous polymer coatings for highly efficient passive daytime radiative cooling. *Science* **362**, 315–319 (2018).

S6. Li T, Zhai Y, He SM et al. A radiative cooling structural material. *Science* **364**, 760–763 (2019).

S7. Wang X, Liu XH, Li ZY et al. Scalable flexible hybrid membranes with photonic structures for daytime radiative cooling. *Adv Funct Mater* **30**, 1907562 (2020).

S8. Zhang HW, Ly KCS, Liu XH et al. Biologically inspired flexible photonic films for efficient passive radiative cooling. *Proc Natl Acad Sci USA*

117, 14657–14666 (2020).

S9. Wang T, Wu Y, Shi L et al. A structural polymer for highly efficient all-day passive radiative cooling. *Nat Commun* **12**, 365 (2021).

S10. Li D, Liu X, Li W et al. Scalable and hierarchically designed polymer film as a selective thermal emitter for high-performance all-day radiative cooling. *Nat Nanotechnol* **16**, 153–158 (2021).

S11. Lin CJ, Li Y, Chi C et al. A Solution-processed inorganic emitter with high spectral selectivity for efficient subambient radiative cooling in hot humid climates. *Adv Mater* **34**, 2109350 (2022).

S12. Wang HD, Xue CH, Ji ZY et al. Superhydrophobic porous coating of polymer composite for scalable and durable daytime radiative cooling. *ACS Appl Mater Interfaces* **14**, 51307–51317 (2022).